J. Fluid Mech. (2005), *vol.* 523, *pp.* 261–275.
DOI: 10.1017/S0022112004002125 Printed in the United Kingdom

The effect of an ambient flow on the spreading of a viscous gravity current

By I. EAMES[1], M. A. GILBERTSON[2] AND M. LANDERYOU[1]

[1]Department of Mechanical Engineering and Mathematics, University College London, Torrington Place, London WC1E 7JE, UK

[2]Department of Mechanical Engineering, Bristol University University Walk, Bristol BS8 1TR, UK

(Received 2 April 2004 and in revised form 3 September 2004)

The influence of an external laminar flow on the spreading of a viscous gravity current moving over a horizontal floor is studied theoretically and experimentally. The viscous stress exerted by the ambient flow drives the viscous gravity current streamwise with a velocity proportional to the local height of the current. The one-way coupling between the ambient flow and the spread of the current is examined. Similarity and numerical solutions are developed to describe viscous gravity currents spreading from line and point sources. An experimental study of the spreading of viscous gravity currents issuing from a point source in a channel flow, for both constant-flux and instantaneous releases, confirms the essential character of this description.

1. Introduction

Viscous buoyancy-driven gravity currents are observed in a wide range of chemical-engineering flows and environmental flows, such as the manufacture of laminated boards where a reacting viscous fluid is introduced onto moving surfaces, or in the context of lava flows down the sides of mountains. (A comprehensive review of gravity currents is given by Huppert 2000.) In many problems, the fluid outside the gravity current may be moving, after having been set in motion either by the gravity current displacing it or because of an external pressure field. The effect of a uniform ambient flow is to advect high-Reynolds-number compositional and particle-driven gravity currents (Hallworth, Hogg & Huppert 1998; Hogg & Huppert 2001*a*,*b*) with an additional velocity proportional to the local ambient flow. But, for viscous gravity currents the ambient flow exerts an interfacial drag on the gravity current, driving the current streamwise. Practical situations in which this occurs are stratified liquid–liquid flows in pipes and the later stages of the development of a gravity current in an ambient flow where the boundary layer thickness is much larger than the size of the viscous current. The aim of this paper is to examine the influence of an ambient laminar flow on the development of a viscous gravity current.

A large number of studies have focused on the spreading of viscous gravity currents. Didden & Maxworthy (1982) studied experimentally the flow of viscous gravity currents moving under free surfaces and over rigid walls, and developed a physical model to explain the observed scalings for the rate of encroachment. Huppert (1982) followed that study with a detailed analysis of planar and axisymmetric viscous gravity current flows and was able to confirm the collapsed scalings of Didden & Maxworthy (1982), in addition to performing additional experiments using silicone

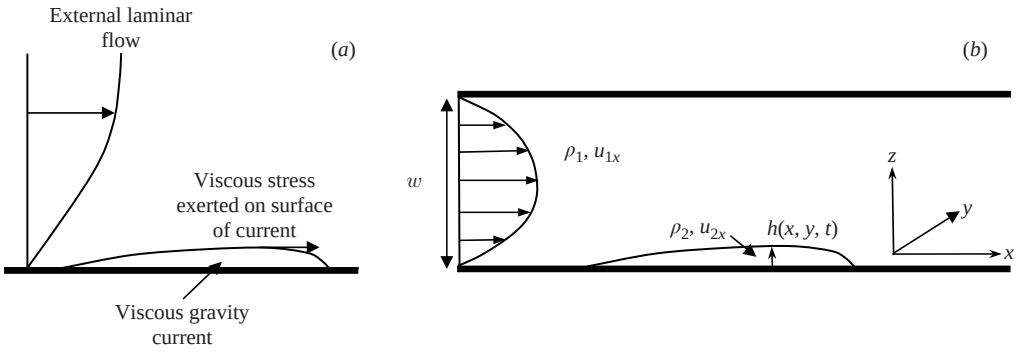

FIGURE 1. A schematic of a viscous gravity current moving in (*a*) an external laminar flow and (*b*) a channel flow, is shown. The gravity current's height is exaggerated.

oils moving in air. Huppert (1982) confirmed that for small Bond numbers, the dynamics of the viscous gravity currents are weakly dependent on complex conditions associated with the contact lines at the nose. Relevant to the work we describe is the detailed analysis by Lister (1992) of gravity currents flowing down inclined walls where, for long time, gravitational acceleration is the main force driving the fluid down the wall. Lister (1992) developed similarity solutions for the spread of gravity currents characterized by low Bond numbers and demonstrated good agreement with his experimental observation.

The aim of this paper is to examine the influence of an external laminar flow on the development of a viscous gravity current moving over a horizontal rigid boundary. We focus on thin viscous gravity currents whose influence on the ambient flow is negligible. The external flow exerts a viscous stress on the surface of the gravity current and drives the current streamwise. The underlying equations developed by coupling mass continuity and momentum equations are reduced to a similarity form and applied to study viscous gravity currents generated by line and point sources. A series of laboratory experiments were undertaken, to test the analysis developed, and these are reported in § 5.

2. Mathematical model

2.1. *Vertically averaged description*

The problem considered is shown schematically in figure 1(*a*), where a viscous gravity current is driven streamwise by an external ambient laminar flow. We first consider a thin gravity current moving in a laminar viscous channel flow (figure 1*b*), before extending the analysis to viscous gravity currents moving in a more general external ambient laminar flow. A viscous liquid (denoted by the subscript 2) is introduced from a source and forms a viscous gravity current in a steady planar channel flow (bounded by walls, separated by a distance w) of a fluid (denoted by the subscript 1). The depth-averaged flow of the ambient fluid is characterized by a mean upstream speed U_f, and driven by a constant pressure gradient $\mathrm{d}P/\mathrm{d}x$.

The viscous forces are assumed to be large compared with inertial forces, and the current is sufficiently shallow for motion perpendicular to the direction of flow of the gravity current to be neglected. The flow is described by Stokes' equation,

$$0 = -\nabla p_i + \mu_i \frac{\partial^2 \boldsymbol{u}_i}{\partial z^2} + \rho_i g \hat{\boldsymbol{z}}, \tag{2.1}$$

for $i = 1, 2$, where $\boldsymbol{u}_i$ is the velocity in fluid i and p_i is the corresponding pressure field, and ρ_i and μ_i are density and viscosity of the fluid respectively. A horizontal constant pressure gradient $\mathrm{d}P/\mathrm{d}x$ is applied to drive the ambient fluid along the channel. The pressures in the two layers of liquid are

$$p_1 = P(x) + \rho_1 g(w - z), \qquad p_2 = P(x) + \rho_1 g(w - h) + \rho_2 g(h - z). \tag{2.2}$$

The horizontal momentum equations can be integrated vertically to obtain

$$\mu_1 u_{1x} = K_1\left[\tfrac{1}{2}(z - w)^2 + a_1(z - w)\right], \qquad \mu_2 u_{2x} = K_2\left[\tfrac{1}{2}z^2 + a_2 z\right], \tag{2.3}$$

where the no-slip conditions ($u_{1x} = 0$ at $z = w$, $u_{2x} = 0$ at $z = 0$) have been applied on the bottom and top of the channel, and

$$K_1 = \frac{\mathrm{d}P}{\mathrm{d}x}, \qquad K_2 = \frac{\mathrm{d}P}{\mathrm{d}x} + (\rho_2 - \rho_1)g\frac{\partial h}{\partial x}. \tag{2.4}$$

The constants a_1 and a_2 are calculated by matching the horizontal component of velocity and the tangential shear stress across the interface between the gravity current and ambient fluid. When the gravity current is thin ($h/w \to 0$), the mean flow of the ambient fluid is unchanged from its upstream value and $a_1 \to w/2$ so that $K_1 = -12U_f\mu_1/w^2$. In this limit, $a_2 \to K_1 w/2K_2$, and the depth-averaged flow in the gravity current tends to

$$\overline{u}_{2x} = \frac{h^2 K_2}{6\mu_2} + \frac{K_1 wh}{4\mu_2} = -\frac{\rho_1 g' h^2}{3\mu_2}\frac{\partial h}{\partial x} + 3\frac{h}{w}\frac{\mu_1}{\mu_2}U_f, \tag{2.5}$$

where $g' = g(\rho_2 - \rho_1)/\rho_1$. In the limit of $h/w \to 0$, the change in u_{1x} is negligible. The form of the driving force could be deduced in a more physical manner by noting that as $h/w \to 0$, the tangential shear stress exerted on the gravity current tends to the shear stress exerted on the channel walls in the absence of the gravity current, $\tau = \mu_1 \mathrm{d}u_{1x}/\mathrm{d}z\|_{z=0}$. The additional effect of the shear stress is to increase the depth-averaged streamwise velocity in the thin gravity current by

$$\frac{h\tau}{2\mu_2} = \frac{h\mu_1}{2\mu_2}\left.\frac{\mathrm{d}u_{1x}}{\mathrm{d}z}\right|_{z=0} = \frac{3U_f h\mu_1}{w\mu_2}. \tag{2.6}$$

Combining (2.5) with the depth-averaged mass conservation equation yields

$$\frac{\partial h}{\partial t} = \frac{\rho_1 g'}{3\mu_2}\frac{\partial}{\partial x}\left(h^3\frac{\partial h}{\partial x}\right) - \frac{\tau}{4\mu_2}\frac{\partial h^2}{\partial x}. \tag{2.7}$$

We study currents generated by a line source when the volume added is qt^α. Equation (2.7) is solved subject to a mass flux condition at the source which is expressed, for a planar flow, in the integral form

$$\int_{-x_T}^{x_N} h\mathrm{d}x = qt^\alpha, \tag{2.8}$$

where the gravity current lies in the region mapped out by $-x_T < x < x_N$.

For a gravity current generated by a point source, we must include the additional cross-flow in the y-direction, $\overline{u}_{2y} = -(\rho g h^2/3\mu_2)\partial h/\partial y$. The flow is described by

$$\frac{\partial h}{\partial t} = \frac{\rho_1 g'}{3\mu_2}\frac{\partial}{\partial x}\left(h^3\frac{\partial h}{\partial x}\right) + \frac{\rho_1 g'}{3\mu_2}\frac{\partial}{\partial y}\left(h^3\frac{\partial h}{\partial y}\right) - \frac{\tau}{4\mu_2}\frac{\partial h^2}{\partial x}. \tag{2.9}$$

The conservation of mass for a planar point source, expressed in an integral form, is

$$\int_{-x_T}^{x_N}\int_{-y_W(x)}^{y_W(x)} h\mathrm{d}y\mathrm{d}x = Qt^{\alpha}, \tag{2.10}$$

where the gravity current lies in the region mapped out by $-x_T < x < x_N$ and $|y| < y_W$.

The form of the above equation is similar to those that describe viscous flows down inclined surfaces where the driving term is proportional to h^2 (Lister 1992) or for viscous flow transported along moving belts, where the driving term is proportional to h^0 (Eames, Gilbertson & Wright 2002). Equation (2.7) is a member of a broad class of nonlinear advection equations and can be analysed in the same way as other similar lubrication equations using the framework of analysis developed by Lister (1992). For a short time or when the viscosity of the ambient fluid is much smaller than the gravity current, the influence of the driving viscous stresses induced by the ambient laminar flow is weak and the resulting equations (2.7) and (2.9) reduce to those discussed and solved by Huppert (1982). Here we strictly focus on the long-time behaviour when the shear stress exerted on the surface of the viscous gravity current is important and the second and third terms in (2.7), or the third and fourth terms in (2.9), are comparable.

3. Similarity solutions for a line source

Equations (2.7) and (2.8) may be non-dimensionalized for a line source by using the scalings $T = t/T^*$, $X = x/X^*$, and $H = h/H^*$ where

$$X^* = \left(\frac{3\mu_2}{\rho_1 g'}\right)^{(\alpha-1)/(\alpha-3)} Q^{-2/(3-\alpha)} \left(\frac{\tau}{4\mu_2}\right)^{(\alpha+1)/(\alpha-2)},$$

$$H^* = Q^{-1/(\alpha-1)} \left(\frac{3\mu_2}{\rho_1 g'}\right)^{(\alpha-1)/(\alpha-3)} \left(\frac{\tau}{4\mu_2}\right)^{(2\alpha-1)/(\alpha-3)},$$

$$T^* = Q^{-1/(\alpha-3)} \left(\frac{\tau}{4\mu_2}\right)^{5/(\alpha-3)} \left(\frac{3\mu_2}{\rho_1 g'}\right)^{2/(\alpha-3)}.$$

This results in

$$\frac{\partial H}{\partial T} = \frac{\partial}{\partial X}\left(H^3\frac{\partial H}{\partial X}\right) - \frac{\partial H^2}{\partial X}, \tag{3.1}$$

and

$$\int_{X_T}^{X_N} H\mathrm{d}X = T^{\alpha}. \tag{3.2}$$

Equation (3.2) possesses similarity solutions of the second kind (Barenblatt 1996) which are derived by employing the transformation $s = \log T$, $\phi = HT^{-(\alpha-1)/2}$ and $\zeta = XT^{-(\alpha+1)/2}$ which reduces (3.1) to

$$\phi_s + \alpha\phi = \left(\tfrac{1}{2}(\alpha+1)\phi\zeta + \phi^3\phi_\zeta - \phi^2\right)_\zeta + \mathrm{e}^{(\alpha-3)s/2}, \tag{3.3}$$

and the integral constraint imposed on the solution is now $\int \phi\mathrm{d}\zeta = 1$. We have restricted our attention to viscous gravity currents which are much thinner than the channel height so that $\alpha \leqslant 1$ and $H^* \ll w$. As $s \to \infty$, the similarity solution of (3.3) ultimately tends to

$$\alpha\phi = \tfrac{1}{2}(\alpha+1)(\phi\zeta)_\zeta - (\phi^2)_\zeta, \tag{3.4}$$

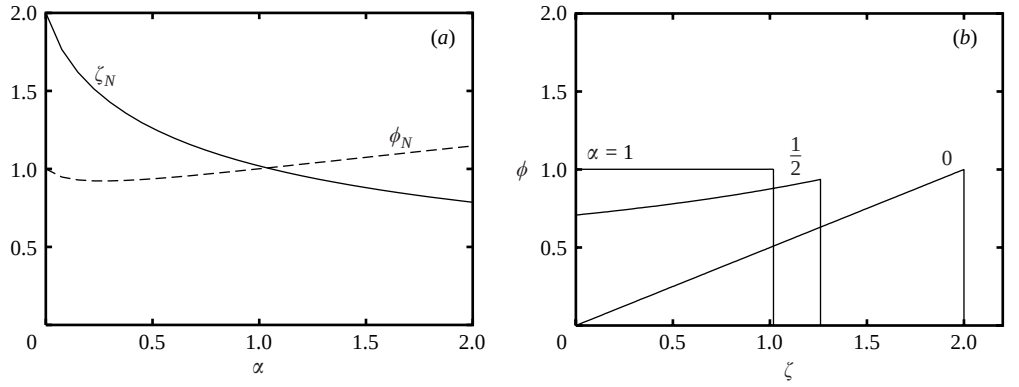

FIGURE 2. (*a*) Height and length of the similarity gravity currents generated by a line source, for different values of α. (*b*) The shape of the gravity current is shown for $\alpha = 0$, $\frac{1}{2}$, and 1.

whose solution is expressed implicitly as

$$\zeta = 2\left(\frac{\phi^{-2/(\alpha-1)} - \phi_0^{-2/(\alpha-1)}}{\phi^{(\alpha+1)/(\alpha-1)}}\right), \tag{3.5}$$

where $\phi_0 = \phi(0)$.

The two conditions which determine the solution are the boundary condition $\phi_0 = \alpha^{1/2}$ (which arises because the flux of fluid is equal to α in dimensionless form) and the integral constraint $\int_0^{\zeta_N} \phi \mathrm{d}\zeta = 1$. Two solutions which may be determined analytically are the case of an instantaneous release of fluid, where

$$\phi(\zeta) = \zeta/2, \qquad \zeta_N = 2, \qquad \phi_N = 1 \qquad (\alpha = 0), \tag{3.6}$$

and the case of a constant-flux source,

$$\phi(\zeta) = 1, \qquad \zeta_N = 1, \qquad \phi_N = 1 \qquad (\alpha = 1). \tag{3.7}$$

The length (ζ_N) and height (ϕ_N) are calculated numerically and are shown in figure 2(*a*). Figure 2(*b*) shows how the long-time similarity solutions vary with α.

It is clear that the gradients of height corresponding to the long-time similarity solutions are infinite at the front and back of the current. This step change was resolved by Lister (1992) for his particular system; the case here differs only in the algebra. The stagnant pond has the form $H(X, T) = [\alpha T^{(\alpha-1)} + X]^{1/2}$, so that for $\alpha < 1$ the stagnant pond is shrinking with time and would tend to leave a wetted surface behind, while for $\alpha = 1$ the pool dimensions do not change. For $\alpha > 1$, the pool dimensions grow and at some time later, the solution becomes inconsistent with the assumption $h/w \ll 1$.

According to (3.3), the nose of the current (in similarity variables) has a length $\mathrm{e}^{(\alpha-3)s/2}$. By transforming into the local coordinates of the gravity current nose (χ, s), where $\chi = (\zeta_N - \zeta)\mathrm{e}^{(-\alpha+3)s}$, the leading-order terms reduce to

$$\tfrac{1}{2}(\alpha+1)\phi_\chi \zeta_N - 2\phi\phi_\chi = (\phi^3\phi_\chi)_\chi. \tag{3.8}$$

Integrating this equation twice, we find that the shape of the fluid layer in the vicinity of the nose is

$$\chi = -\phi_N^2 \log\left(1 - \frac{\phi}{\phi_N}\right) - \phi_N\phi - \tfrac{1}{2}\phi^2, \tag{3.9}$$

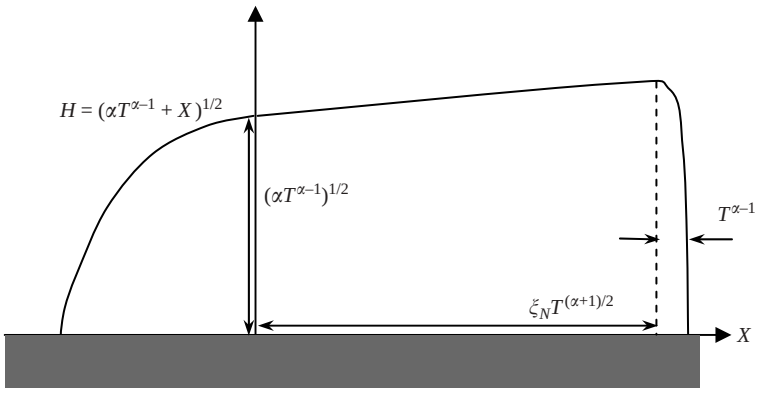

FIGURE 3. Schematic showing the length scales associated with the near-source region, the far-field region and the boundary layer at the front of the current.

where $\phi_N = (\alpha + 1)\zeta_N/2$ and the condition $\phi = 0$ at $\chi = 0$ is applied (see figure 3). Thus according to the above expression, as $\chi \to \infty$, the similarity height ϕ tends to ϕ_N, matching the main body of the flow. As noted by Huppert (1982) and Lister (1992), the details of the flow in the vicinity of the nose of the current have a relatively weak influence on the overall dynamics of the gravity current.

4. Similarity solutions for point sources ($0 \leqslant \alpha \leqslant 3/2$)

We proceed to develop the analysis to include gravity currents issuing from a point source. Equations (2.10) and (2.9) can be non-dimensionalized using $T = t/T^*$, $X = x/X^*$, $Y = y/Y^*$ and $H = h/H^*$, where

$$T^* = \left(\frac{\rho_1 g'}{3\mu_2}\right)^{3/(5-\alpha)} \left(\frac{\tau}{2\mu_2}\right)^{-8/(5-\alpha)} Q^{1/(5-\alpha)},$$

$$X^* = Y^* = \left(\frac{\rho_1 g'}{3\mu_2}\right)^{(1+\alpha)/(5-\alpha)} \left(\frac{\tau}{2\mu_2}\right)^{-(3\alpha+1)/(5-\alpha)} Q^{2/(5-\alpha)},$$

$$H^* = \left(\frac{\rho_1 g'}{3\mu_2}\right)^{-2/(5-\alpha)} \left(\frac{\tau}{2\mu_2}\right)^{-2(1-\alpha)/(5-\alpha)} Q^{1/(5-\alpha)}.$$

Application of these scalings gives the conservation equations for the gravity current the forms

$$\frac{\partial H}{\partial T} = \frac{\partial}{\partial Y}\left(H^3 \frac{\partial H}{\partial Y}\right) + \frac{\partial}{\partial X}\left(H^3 \frac{\partial H}{\partial X}\right) - \frac{\partial H^2}{\partial X}, \tag{4.1}$$

and

$$\int_{X_T}^{X_N} \int_{-Y_W(X)}^{Y_W(X)} H \mathrm{d}Y \mathrm{d}X = T^\alpha. \tag{4.2}$$

where $H = 0$ at $Y = \pm Y_W(X)$.

4.1. *Near-source structure*

The near-source flow is controlled by the instantaneous flux out of the source. Rescaling the characteristic height, length and width of the current as $\mathscr{H} = H/L_H$,

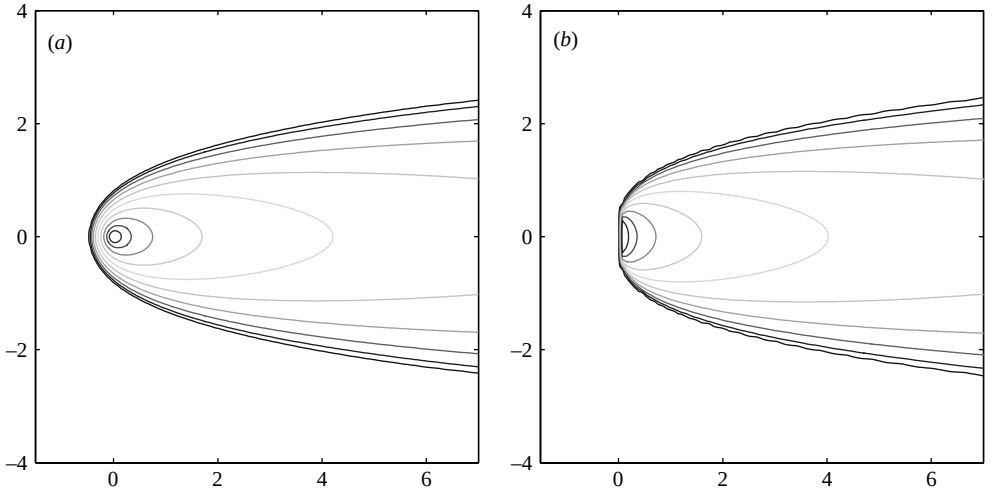

FIGURE 4. Comparison between (*a*) the steady near-source similarity solution (satisfying (4.3)), determined numerically, and (*b*) the analytical approximation (4.5), plotted as a function $\mathscr{X}$, $\mathscr{Y}$. The contours correspond to dimensionless height $\mathscr{H} = 0.1$ to 1, in increments of 0.1.

$\mathscr{X} = X/L$, $\mathscr{Y} = Y/L$ where $L_H = (\alpha T^{\alpha-1})^{1/2}$ and $L = L_H^2$, the local dynamics of the gravity current are described by

$$\frac{\partial}{\partial \mathscr{Y}}\left(\mathscr{H}^3\frac{\partial \mathscr{H}}{\partial \mathscr{Y}}\right) + \frac{\partial}{\partial \mathscr{X}}\left(\mathscr{H}^3\frac{\partial \mathscr{H}}{\partial \mathscr{X}}\right) - \frac{\partial \mathscr{H}^2}{\partial \mathscr{X}} = O\left(T^{(\alpha-3)/2}\right), \tag{4.3}$$

where the similarity variables $\mathscr{H}$, $\mathscr{Y}$ and $\mathscr{X}$ are order unity. The similarity solution (4.3) is independent of α (for $\alpha < 3$). Figure 4(*a*) shows a numerical solution to (4.3), where a constant-flux source is introduced at the origin. The analysis breaks down close to the origin (as $\mathscr{X}, \mathscr{Y} \to 0$) because the source flow leads to a singularity in the height of the form $\mathscr{H} \sim (\log(\mathscr{X}^2 + \mathscr{Y}^2))^{1/2}$; this is reconciled physically because the source issues from a finite area. As with the line source problem, the near-source flow needs to be matched onto an advancing contact line for $\alpha > 1$ or a draining film for $\alpha < 1$.

Far downstream of the source ($\mathscr{X} \to \infty$), the similarity solution asymptotes to

$$\frac{\partial}{\partial \mathscr{Y}}\left(\mathscr{H}^3\frac{\partial \mathscr{H}}{\partial \mathscr{Y}}\right) = \frac{\partial \mathscr{H}^2}{\partial \mathscr{X}}, \qquad \int_{-\mathscr{Y}_W}^{\mathscr{Y}_W} \mathscr{H}^2 \mathrm{d}\mathscr{Y} = 1, \tag{4.4}$$

which describes physically a balance between cross-slope spreading by gradients of hydrostatic pressure and advection by the laminar mean flow. The similarity solution to (4.4),

$$\mathscr{H} = \frac{3^{1/6}}{\mathscr{X}^{1/6}2^{2/3}}\left(1 - \frac{\mathscr{Y}^2}{(9\mathscr{X}/4)^{2/3}}\right)^{1/2}, \tag{4.5}$$

is plotted in figure 4(*b*) and compares favourably with the numerical solution to (4.3), shown in figure 4(*a*). According to (4.5), the width of the gravity current is $\mathscr{Y}_W = (9\mathscr{X}/4)^{1/3}$.

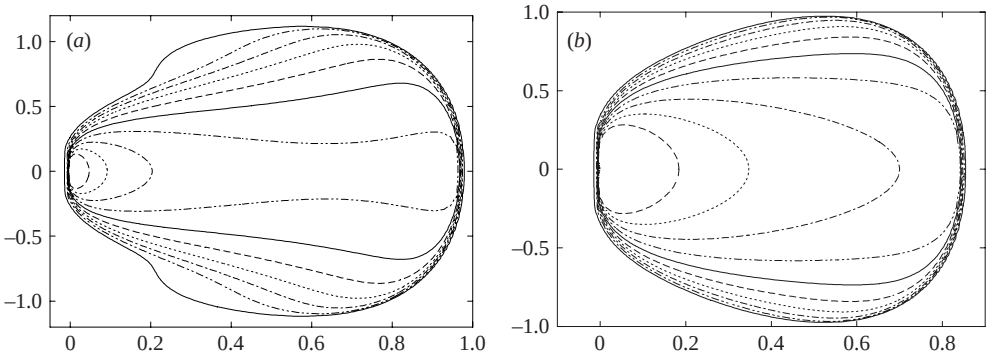

FIGURE 5. The similarity solutions to (4.7) for (*a*) $\alpha = 0.5$ and (*b*) $\alpha = 1$. The contours correspond to dimensionless height $\phi = 0.1$ to 1, in increments of 0.1.

4.2. *Similarity solution* $(1/3 < \alpha \leqslant 3/2)$

Similarity solutions of (4.1) and (4.2) of the second kind (Barenblatt 1996) can be obtained by using the transformations $s = \log T$, $\phi = HT^{-(2\alpha-3)/7}$, $\zeta = XT^{-(2\alpha+4)/7}$ and $\eta = YT^{-(3\alpha-1)/7}$. From the transformations, it is clear that in order for the model to be consistent with the assumption than the gravity current is thin relative to the channel height, a necessary condition is that $\alpha \leqslant 3/2$. The mass flux constraint reduces to

$$\iint \phi \mathrm{d}\eta \mathrm{d}\zeta = 1, \tag{4.6}$$

and the momentum equation becomes

$$\phi_s + \alpha\phi = \left(\frac{(2\alpha+4)}{7}\phi\zeta - \phi^2\right)_\zeta + \left(\frac{(3\alpha-1)}{7}\phi\eta + \phi^3\phi_\eta\right)_\eta + \mathrm{e}^{(2\alpha-10)s/7}(\phi^3\phi_\zeta)_\zeta. \tag{4.7}$$

The length and width of the current in similarity form, ζ_N and η_W respectively, are related to the dimensionless length and half-width through

$$X_N(T) = \zeta_N(s)T^{(2\alpha+4)/7}, \qquad Y_W(T) = \eta_W(s)T^{(3\alpha-1)/7}. \tag{4.8}$$

Analysis of (4.7) shows that for $\alpha > 1/3$, the cross-stream diffusive flux of fluid $(-\phi^3\phi_\eta)$ is balanced by the inward $-(3\alpha-1)\phi\eta/7$ flux, so that ϕ tends to a constant solution as $s \to \infty$. The long-time similarity solution then satisfies

$$\alpha\phi = \frac{\partial}{\partial\zeta}\left(\frac{(2\alpha+4)}{7}\phi\zeta - \phi^2\right) + \frac{\partial}{\partial\eta}\left(\frac{(3\alpha-1)}{7}\phi\eta + \phi^3\phi_\eta\right). \tag{4.9}$$

However, for $\alpha \leqslant 1/3$, the similarity solution grows with time and we must resort to a blend of numerical solution and asymptotics.

Numerical solutions to the above equation were developed by introducing a source of strength α at the origin $(\eta, \zeta) = (0, 0)$. The strength of the source was set to ensure that as $s \to \infty$, the volume of fluid deposited is unity. Equation (4.7) was solved using a finite difference scheme, explicit in time, second-order accurate in space, that employed the Il'lin scheme (Clauser & Kiesner 1987). Numerical viscosity was added in the ζ-direction to smooth out oscillations.

For $1/3 < \alpha \leqslant 3/2$, the similarity solution ultimately tends to a steady state. Two representative similarity solutions are plotted in figure 5. The ultimate length and

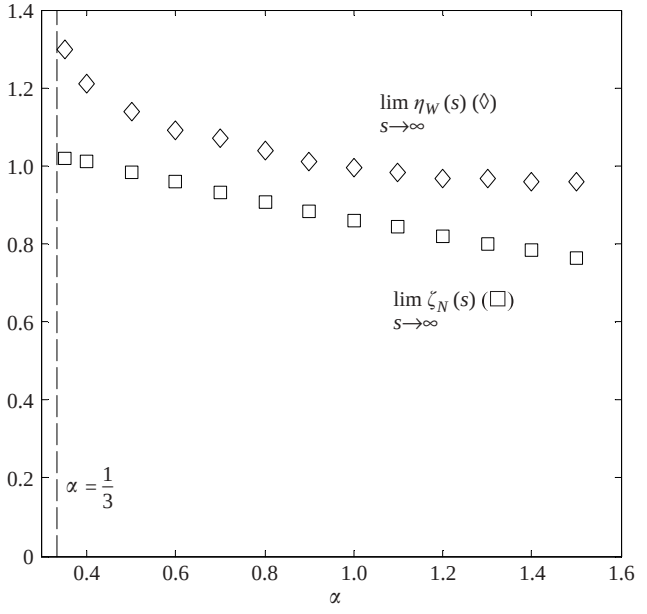

FIGURE 6. The ultimate length and half-width of the gravity current in similarity form (from (4.7)), are shown as functions of α for $1/3 < \alpha \leqslant 3/2$. For $0 \leqslant \alpha \leqslant 1/3$ the similarity solution does not approach a steady state.

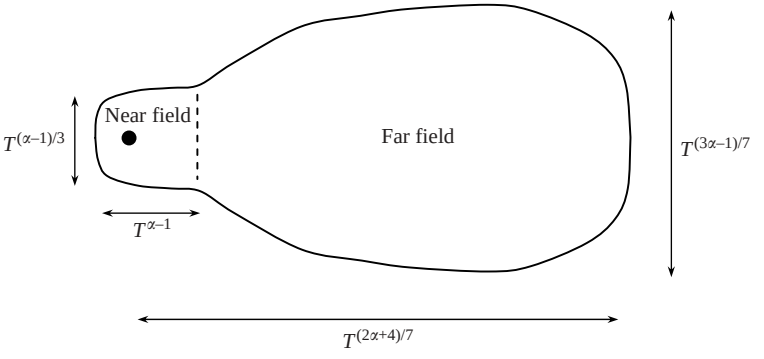

FIGURE 7. Schematic of the spreading of fluid from a point source for $1/3 < \alpha \leqslant 3/2$.

half-width of the similarity solution, $\lim_{s\to\infty} \zeta_N$ and $\lim_{s\to\infty} \eta_W$, for $1/3 < \alpha < 3/2$, are shown in figure 6. The corresponding dimensionless length and half-width can be obtained from (4.8). A schematic of the characteristic scales of the flow is shown in figure 7.

4.2.1. *Similarity solution for* $\alpha = 0$

When $\alpha \leqslant 1/3$ the cross-flow flux of fluid (the second term on the right-hand side of (4.7)) is unbalanced and the width of the current, η_W, in terms of the similarity variables, increases with time. Here we proceed to develop an asymptotic model for $\alpha = 0$, corresponding to an instantaneous release of fluid.

When a fixed volume of dense fluid is released into a channel flow, we anticipate that the width of the current ultimately tends to a fixed value with increasing time because

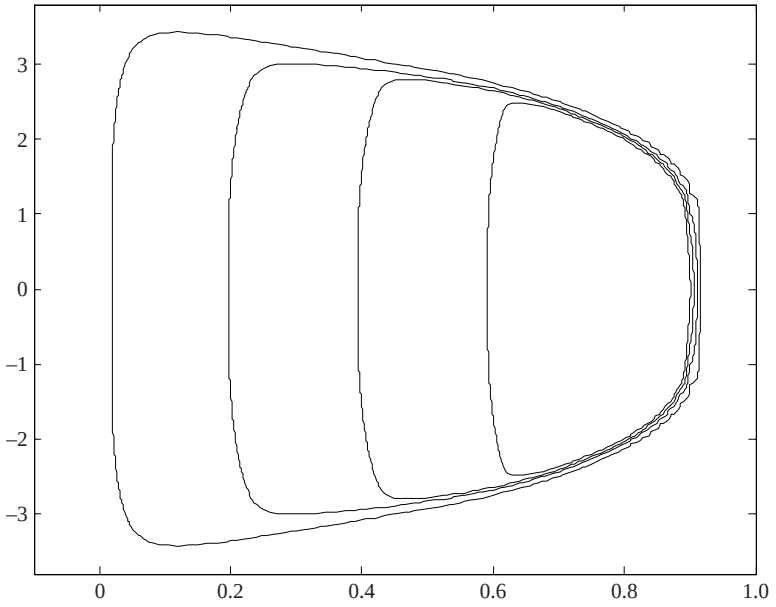

FIGURE 8. Similarity solution ϕ for $\alpha = 0$ at $s = 4.5$.

cross-stream gradients in hydrostatic pressure are rapidly reduced as the current spreads in the streamwise direction. From (4.8) the dimensionless half-width of the gravity current is $Y_W \sim \eta_W(s)T^{-1/7}$, and so we anticipate that ultimately $\eta_W \sim \mathrm{e}^{s/7}$. This is confirmed by the detailed analysis below.

Numerical solutions to (4.7) were obtained by initializing the flow with a unit volume of fluid, and integrating. We shall show that as $s \to \infty$, the flow occupies the region $0 < \zeta < \zeta_P$ where ζ_P is of the form

$$\zeta_P(\eta, s) = \zeta_N(s) f\left(\eta/\eta_W(s)\right), \qquad |\eta| \leqslant \eta_W(s), \tag{4.10}$$

where f, $\zeta_N(s)$ and $\eta_W(s)$ are to be determined. As shown in figure 8, the flow (in the similarity variables) is one in which contours of ϕ are essentially parallel to the front in the boundary layer, and there is a rapid change in ϕ across the boundary layer. Within the core of the flow, $\phi = \frac{4}{7}\zeta$. The total flux in the η-direction is estimated to be

$$F(\eta, s) = \int_0^{\zeta_P} \left(\frac{1}{7}\phi\eta - \phi^3\phi_\eta\right) \mathrm{d}\zeta = \frac{2}{49}\zeta_P^2\eta - \frac{\phi_N^4}{4}\frac{\partial \zeta_P}{\partial \eta}. \tag{4.11}$$

The flux of fluid in the η-direction at a lateral position η' is equal to the rate of decrease of the volume of fluid in the region $0 < \eta < \eta'$, thus

$$F(\eta, s) = -\frac{\partial}{\partial s}\left(\frac{2}{7}\zeta_N^2\eta_W \int_0^{\eta/\eta_W} \{f(u)\}^2 \mathrm{d}u\right) = \eta\frac{2}{7}\zeta_P^2\frac{\dot{\eta}_W}{\eta_W}. \tag{4.12}$$

Equating (4.11) and (4.12) and integrating with respect to η gives

$$\frac{1}{49}\eta^2 - \frac{64}{7203}\zeta_P^3 = \frac{1}{7}\eta^2\frac{\dot{\eta}_W}{\eta_W} + c(s), \tag{4.13}$$

where the constant of integration $c(s)$ is determined from the requirement that $\zeta_P = 0$ when $\eta = \eta_W$. Thus,

$$f(u) = (1-u^2)^{1/3}, \qquad \zeta_N = \left[\frac{1029}{64}\left(\dot{\eta}_W \eta_W - \frac{1}{7}\eta_W^2\right)\right]^{1/3}. \tag{4.14}$$

The volume of fluid released to form the gravity current is unity (see (4.6)), so that

$$\zeta_N^2 \eta_W = \frac{7}{4\displaystyle\int_0^1 \{f(u)\}^2 \mathrm{d}u} = \frac{7(\frac{4}{3}!)}{4\left(2^{2/3}\right)\left(\frac{1}{3}!\right)^2} = \mathscr{C} \approx 2.368. \tag{4.15}$$

Combining the above expressions and integrating,

$$\eta_W(s) = \left[\mathrm{e}^{s/2}\left[\eta_W^{7/2}(0) + \frac{64\mathscr{C}^{3/2}}{147}\right] - \frac{64\mathscr{C}^{3/2}}{147}\right]^{2/7}, \tag{4.16}$$

where the half-width at $s = 0$ is $\eta_W(0)$. For $s \gg 1$ and $\eta_W(0) = 0$ the length and half-width, in similarity form, tend to

$$\zeta_N \sim 1.44\,\mathrm{e}^{-s/14}, \qquad \eta_W \sim 1.14\,\mathrm{e}^{s/7}, \tag{4.17}$$

which in dimensionless variables yields

$$X_N \sim 1.44 T^{1/2}, \qquad Y_W \sim 1.14. \tag{4.18}$$

Thus the length grows diffusively with time and the width ultimately tends to a constant width. Equation (4.16) shows that the coefficients in (4.18) depend exactly on how the numerical solutions are initialized. The essential character of the asymptotic analysis is confirmed both numerically and experimentally in the next section.

5. Experimental study

To illustrate experimentally how a laminar ambient flow affects the spreading of a viscous gravity current, we consider viscous gravity currents introduced into a channel flow. A uniform ambient flow of water was generated in a wide long narrow cell (length 90 cm, width 61 cm and wall separation $w = 1.0$ cm). The ambient flow through the channel was driven by a header tank through a flow meter and then a flow calming section which ensured that the flow was steady and laminar. The Reynolds number, $Re = wU_f/\nu$, was in the range of 20–100, which is sufficiently small to ensure that the flow was laminar. Although the flow is not viscously dominated, the departure from a parabolic profile is not severe. But, more importantly, up to $Re \sim 1000$ (White 1998, p. 338) the wall shear stress τ, is sufficiently close to the viscous prediction of $\tau = 6U_f\mu_1/w$ for the experiments to be consistent with the model developed. To eliminate capillary effects, the gravity currents were generated using a saline solution fed from a header tank. Under these conditions, the kinematic viscosity of the gravity current and ambient fluid were assumed to be the same. The entrance to the source has an internal diameter of 0.4 cm and was flush with the channel floor. Care was required to ensure that the temperature of the channel flow water and gravity current water was the same.

A small quantity of fluorescein dye was added to the source fluid to enable the gravity current to be observed. Two types of experiments were undertaken: a constant-flux release from a localized source, and an instantaneous release of fluid. For a constant-flux release, the volume flux was measured from the loss of fluid from

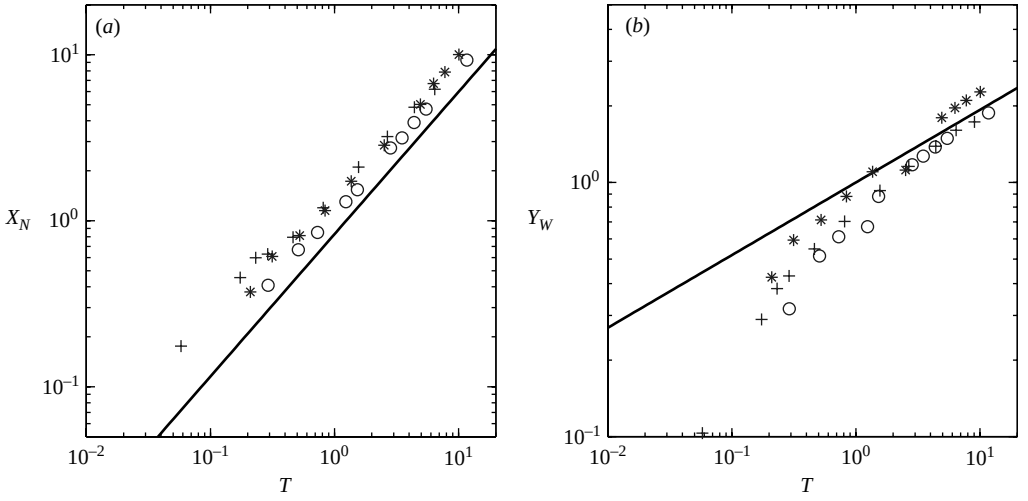

FIGURE 9. Experimental measurements of (*a*) length and (*b*) half-width of a gravity current generated from a constant-volume flux issuing from a point source. The fluid density $(\rho_2 - \rho_1)/\rho_1 = 0.022$ and the mean flow $U_f = 0.91\,\mathrm{cm\ s^{-1}}$, are fixed for each of the experiments. The symbols correspond to a volume flow rate $Q = 0.67\,\mathrm{cm^3\ s^{-1}}$ (+); 0.27 (○); 0.062 (∗). The full lines in (*a*) and (*b*) correspond to the similarity solutions $X_N = 0.83T^{6/7}$ and $Y_W = 1.0T^{2/7}$ respectively.

the header tank; for the instantaneous release experiments, fluid was injected over a short time using a syringe.

5.1. *Constant flux from point source* ($\alpha = 1$)

For a short time, the gravity current was observed to increase in length as it was advected downstream, and spread across-stream by gradients of hydrostatic pressure. The width and length of the gravity current were measured as a function of time from video film. The experimental measurements were rendered dimensionless using the characteristic scales, X^* and T^*, introduced in § 4.

Some of the flow features observed, such as the formation of the fingers, are a common feature of gravity currents moving through less dense fluid and are not a feature of the model developed. Light fluid is trapped near the surface of the channel which rises up through dense gravity currents, creating long thin filaments whose separation scales with the gravity current thickness (Synder & Tait 1998). The effect of the fingers was to increase the thickness of the current and caused the front to be transported slightly faster than the rest of the current. The filaments were ignored in measurements of the length of the current – this was achieved by thresholding the intensity of the digitized images.

Figure 9 shows the variation of the length and width of the gravity current as a function of time, along with the prediction of the similarity solution corresponding to $\alpha = 1$. The agreement between X_N and theoretical predictions is satisfactory. Since the width of the current grows slowly with downstream distance and the length of the channel is only two decades larger than the source size, the finite size of the source appears to dominate the sideways growth of the gravity current. Nevertheless, quantitative agreement is fair. After some time, the near-source behaviour tends to a steady state and the shape of the edge of the current was measured. Figure 10(*a*)

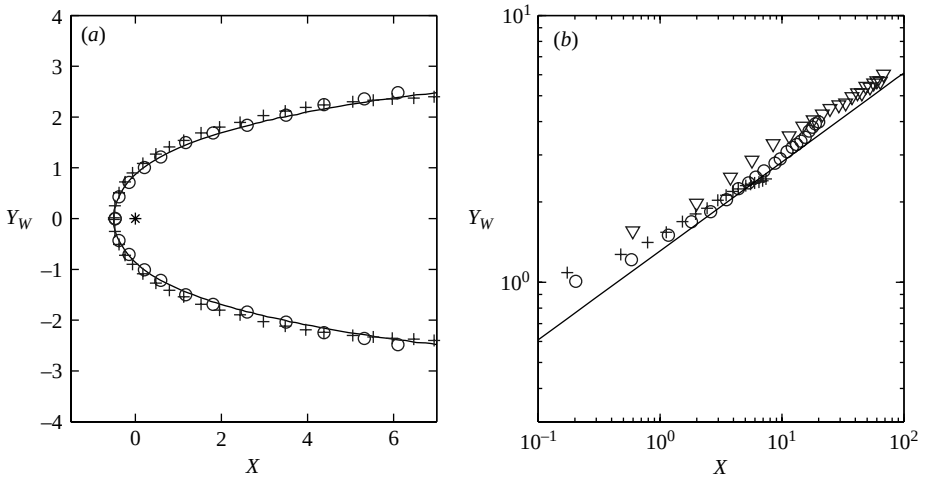

FIGURE 10. Comparison between experimental measurements and numerical solution of (*a*) the shape of the near-source gravity current and (*b*) the half-width of the gravity current as a function of downstream distance. The measurements are made for a constant-flux gravity current. The density of the source fluid and the rate at which is it introduced, were fixed at $(\rho_2 - \rho_1)/\rho_1 = 0.022$ and $Q = 0.031$ cm^3 s^{-1} respectively. The symbols correspond to $U_f =$ 2.1 cm s^{-1} (∇); 0.22 (+); 0.61 ($\circ$). The $*$ symbol in (*a*) denotes the position of the source.

shows a comparison between the numerical solution and experimental measurements of the near-source behaviour of the current and good quantitative agreement is observed. The width of the current as a function of downstream distance is shown in figure 10(*b*), and the similarity prediction, that $Y_W = (9X/4)^{1/3}$ (from (4.6)), is confirmed.

5.2. *Instantaneous release of fluid* ($\alpha = 0$)

The generation of an instantaneous release of fluid into the channel flow, corresponding to $\alpha = 0$, was achieved by rapidly introducing a finite quantity of dense fluid. The thin gravity current initially spread because of buoyancy forces, but the effect of the ambient flow was to stretch the current sufficiently rapidly for cross-stream transport to be quickly inhibited. As with the constant-flux experiments, finger-like intrusions were clearly observed and these were seen at later time to be advected more quickly than the current downstream. The width and length of the current (X_N, Y_W) were measured by thresholding the intensity of the images to ensure the spurious effect of the fingers was ignored.

A comparison between the experimental measurements and predictions for $\alpha = 0$, are shown in figure 11. The scaling of the length, $X_N \sim T^{1/2}$ is adequately reproduced, but the leading coefficient systematically differs by 30% from the theoretical prediction. An analysis of the numerical solutions for $\alpha = 0$, showed that the eventual growth rate of the leading-order coefficient is sensitive to the initial size of the gravity current and how the fluid is introduced. The offset between the numerical predictions, the analytical model and experiments is related to how the gravity current is initially introduced into the flow.

Figure 11(*b*) shows that the width ultimately tends to a constant value, as the longitudinal stretching of the current rapidly diminishes the height of the current and

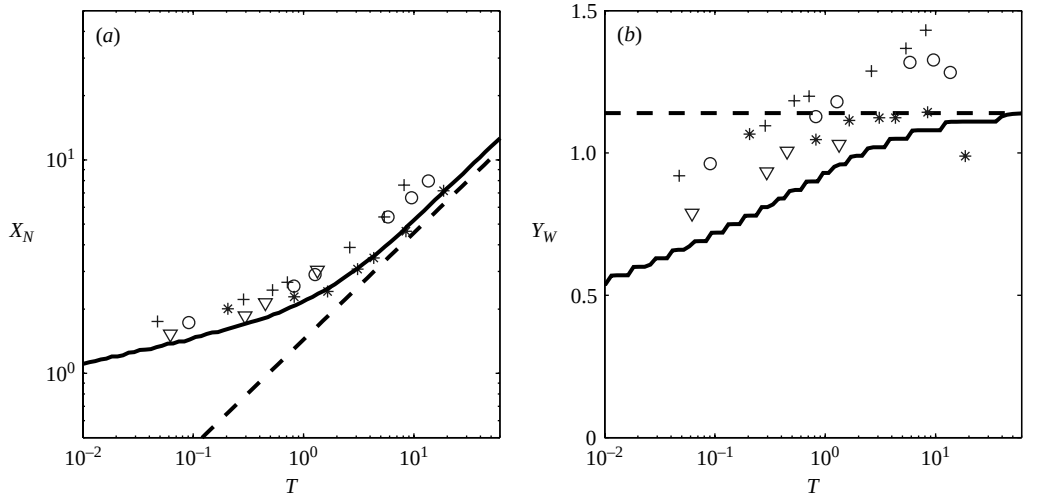

FIGURE 11. Experimental measurements of (*a*) the length X_N and (*b*) the half-width Y_W of a viscous gravity current generated by an instantaneous release of dense fluid. The fluid density and the volume released were fixed at $(\rho_2-\rho_1)/\rho_1 = 0.080$ and 2 cm^3 respectively. The symbols correspond to different mean velocities: $U_f = 2.3$ cm s^{-1} (∗); 1.4 (○); 0.91 (+); 0.23 (▽). The full lines correspond to the length and half-width of the numerical solutions to (4.7) for $\alpha = 0$, while the dashed line corresponds to the approximation (4.18).

	X, Y	H	Comment
Planar source	$T^{(2\alpha+4)/7}$, $T^{(3\alpha-1)/7}$	$T^{(2\alpha-3)/7}$	$1/3 < \alpha \leqslant 3/2$
	$T^{1/2}$, T^0	$T^{-1/2}$	$\alpha = 0$
Line source	$T^{(\alpha+1)/2}$	$T^{(\alpha-1)/2}$	$0 \leqslant \alpha \leqslant 1$

TABLE 1. Summary of characteristic scales of the viscous gravity current. When $\alpha > 3/2$ and >1, for planar and line sources respectively, the height of the viscous gravity current will be so large that it will be incompatible with the modelling assumptions. For planar sources and $0 < \alpha \leqslant 1/3$, the size of the gravity current must be determined numerically.

inhibits cross-stream spreading. The slight decrease in the half-width of the current is related to thresholding the intensity of captured images, particularly when the gravity current was very thin. A numerical solution to (4.7) is also shown in figure 11.

6. Discussion

The influence of an ambient flow on the spreading of a viscous gravity current fundamentally differs from how a high-Reynolds-number gravity current spreads. Rather than the ambient flow only advecting the gravity current (Hallworth *et al.* 1998; Hogg & Huppert 2001*a*,*b*), it exerts a viscous stress on the surface of the current, driving it streamwise. This leads to an additional term in the nonlinear advection equation which ultimately dominates the rate of spreading. A summary of our main results for the characteristic scales of the viscous gravity current is shown in table 1.

The main assumption of the analysis is that the gravity current height is smaller than the boundary layer thickness of the steady ambient laminar flow and a constant viscous stress is exerted on the viscous gravity current. The gravity current was

assumed not to affect the ambient flow so that the streamlines in the ambient flow are not deflected around the gravity current. This places stringent limits on the applicability of the analysis to $0 \leqslant \alpha \leqslant 1$ for planar currents and $0 \leqslant \alpha < 3/2$ for currents issuing from point sources. When $0 \leqslant \alpha \leqslant 1/3$, the similarity analysis presented for point-source releases breaks down and a singularity analysis of the similarity equations must be developed. We have presented an analysis corresponding to an instantaneous release of fluid ($\alpha = 0$).

To test the analysis, we measured how viscous gravity currents spread in a channel flow, where the experimental conditions are consistent with the modelling assumptions. The laboratory measurements for constant-flux releases issuing from a point ($\alpha = 1$) and instantaneous releases ($\alpha = 0$) are in good agreement with the theoretical and numerical predictions. The main difference between the experimental and theoretical predictions appear to be due to the sensitivity of the leading-order coefficients to the initial, finite size of the gravity current.

This project arose through a Royal Society Equipment Grant to examine 'Dispersion in porous media' at the School of Mathematics, Bristol University.

REFERENCES

Barenblatt, G. I. 1996 *Scaling, Self-similarity, and Intermediate Asymptotics*. Cambridge University Press.

Clauser, C. & Kiesner, S. 1987 A conservative, unconditionally stable, second-order three-point differencing scheme for the diffusion-convection equation. *Geophys. J. R. Astron. Soc.* **91**, 557–568.

Didden, N. & Maxworthy, T. 1982 The viscous spreading of planar and axisymmetric gravity currents. *J. Fluid Mech.* **121**, 27–42.

Eames, I., Gilbertson, M. A. & Wright, N. 2002 Fluid mechanics of insulation board manufacture. *AIChE. J.* **48**, 2481–2491.

Hallworth, M. A., Hogg, A. J. & Huppert, H. E. 1998 Effects of external flow on compositional and particle gravity currents. *J. Fluid Mech.* **359**, 109–142.

Hogg, A. J. & Huppert, H. E. 2001*a* Two-dimensional and axisymmetric models for compositional and particle-driven gravity currents in uniform ambient flows. In *Sediment Transport and Deposition by Particulate Gravity Currents*. Spec. Publs. Intl. Ass. Sediment, vol. 31, pp. 121–134.

Hogg, A. J. & Huppert, H. E. 2001*b* Spreading and deposition of particulate matter in uniform flows. *J. Hydraul. Res.* **39**, 505–518.

Huppert, H. E. 1982 The propagation of two-dimensional and axisymmetric viscous gravity currents over a rigid horizontal surface. *J. Fluid Mech.* **121**, 43–58.

Huppert, H. E. 2000 Geological fluid mechanics. In *Perspectives in Fluid Dynamics: A Collective Introduction to Current Research* (ed. G. K. Batchelor, H. K. Moffatt & M. G. Worster), pp. 447–506, Cambridge University Press.

Lister, J. 1992 Viscous flows down an inclined plane from point and line sources. *J. Fluid Mech.* **242**, 631–654.

Snyder, D. & Tait, S. 1998 A front flow instability in viscous gravity currents. *J. Fluid Mech.* **369**, 1–21.

White, F. M. 1998 *Fluid Mechanics*, 4th Edn. McGraw Hill.